UDK 621.791.725:622'18:669.15:519.61
Original scientific article/Izvirni znanstveni članek

ISSN 1580-2949
MTAEC9, 55(3)411(2021)

NUMERICAL STUDY OF THE TEMPERATURE FIELD FOR Fe_3Al LASER WELDING

NUMERIČNA ŠTUDIJA TEMPERATURNEGA POLJA LASERSKO VARJENEGA Fe_3Al

Josef Bradáč[1*], Jiří Hozman[2], Jan Lamač[3]

[1]Technical University of Liberec, Faculty of Mechanical Engineering, Studentská 1402/02, 461 17, Liberec, Czech Republic
[2]Technical University of Liberec, Faculty of Science, Humanities and Education, Studentská 1402/02, 461 17, Liberec, Czech Republic
[3]CTU in Prague, Faculty of Civil Engineering, Thákurova 7, 166 29 Prague, Czech Republic

Prejem rokopisa – received: 2020-09-18; sprejem za objavo – accepted for publication: 2021-03-11

doi:10.17222/mit.2020.185

The main objective of this paper was focused on a numerical study related to a proper evaluation of the temperature field during the laser-welding process. The investigated material used for the experiments was Fe_3Al, given its properties and promising application potential. The original experiment was based on a 3D model of a butt weld. However, to reduce the computational complexity, a planar variant of the heat-transfer equation with suitable choices of surface and volumetric heat sources, given by modified Gaussian pulses, is used to model the temperature distribution in the fixed cross cut during the laser welding. Subsequently, the numerical scheme based on the discontinuous Galerkin method was employed to evaluate the temperature field more properly and to identify the main characteristics of the molten zone. Finally, the numerical study was performed for various combinations of the welding parameters, such as laser-beam power and welding speed. The obtained results were in good agreement with the expected behavior, and thus illustrate the optimization potential of the proposed numerical scheme in the similar issues of a laser-welding processes.

Keywords: iron aluminide, laser welding, temperature field, numerical simulation

Glavni predmet raziskave v članku je bil osredotočen na numerično študijo, ki lahko ustrezno ovrednoti temperaturno polje, nastalo med laserskim varjenjem. Avtorji so za svoje eksperimentalne raziskave uporabili železov aluminid (Fe_3Al), ki predstavlja nov obetajoč material za različne aplikacije. Originalni preizkus je temeljil na 3D modelu čelnega vara. Vendar pa so morali, zaradi računalniške kompleksnosti problema, za uporabljeni model temperaturne porazdelitve fiksnega prečnega preseka med laserskim varjenjem, izbrati ravninsko varianto enačbe za prenos toplote s površinskimi in volumskimi izvori toplote podanimi z modificiranimi Gaussianovimi pulzi. Naslednji korak je bila uporaba numerične sheme na osnovi Galerkinove metode za boljše ovrednotenje temperaturnega polja in identifikacijo glavnih značilnosti raztaljene cone. Avtorji so ob zaključku izvedli še numerično študijo za različne kombinacije parametrov varjenja, kot so na primer različne moči laserskega snopa in hitrosti varjenja. Dobljeni rezultati so se dobro ujeli s pričakovanji in na ta način se je dokazal optimizacijski potencial predlagane numerične sheme za podobne izbrane razmere laserskega varjenja.

Ključne besede: železov aluminid, lasersko varjenje, temperaturno polje, numerična simulacija

1 INTRODUCTION

The requirements for the quality, efficiency and sustainability of the manufacturing processes are ever more demanding nowadays, calling for the employment of new, special technologies and unconventional materials. Intermetallic compounds can be considered as unconventional and progressive materials. Generally, the most important of the intermetallic compounds are nickel, titanium and iron aluminides. Some of them have been already used in industrial practice, others are objects of application research. Deeper investigations of iron aluminides as intermetallic compounds began in 1990s, when their excellent corrosion resistance was discovered.[1,2]

The advantage of iron aluminides is the relatively low material cost together with the saving of elements as standard guaranteeing corrosion resistance of materials such as Cr, Ni.[3] Another advantage is their low specific weight, lower than that of high-alloy steel, which is very important since the demands on weight reduction of machines and components are ever growing. The tensile strength of iron aluminides is comparable to standard steel types. Iron aluminides are further characterized by their resistance to cavitation, wear resistance and excellent resistance to environments containing sulfur and its compounds.[4] For these reasons, their use falls within the area of structural components in the power industry, such as heaters, heat exchangers and equipment for the chemical industry. Also, they can be used for turbine and compressor components, combustion and jet engines, components of nuclear reactors, generator plates, etc.

The disadvantages of iron aluminides include complicated manufacture and processing associated with the mechanical and thermal-physical properties of these materials. The main problem is especially their high brittleness at normal temperature, which causes considerable problems in forming and welding.[5] Forming is thus pos-

*Corresponding author's e-mail:
josef.bradac@tul.cz (Josef Bradáč)

sible in principle only at high temperatures and the weldability becomes very difficult, especially when using conventional welding methods.

For this reason, the application of unconventional welding techniques and the use of numerical analysis enabling a detailed study of the welding process can be a possible solution to the problem. Unlike a huge number of articles devoted to the numerical simulation of laser welding purely from the point of view of the user of a commercial software (e.g., SYSWELD), we intend to introduce the problem to the readers in much more detail in terms of the mathematical modelling and its numerical implementation, including the use of open-source software, because these aspects are not usually emphasized.

The core of the paper is organized as follows. In Section 2 we introduce the relevant Fe_3Al material properties. Section 3 and Section 4 present the planar mathematical model and its numerical treatment respectively. Finally, in Section 5, the results obtained from the numerical study demonstrate the capabilities of the proposed approach, followed by a broader discussion.

2 MATERIAL

An iron aluminide alloy was used as the basic material for further numerical study. The chemical composition is Fe 79.53 *w*/%, Al 16.2 *w*/%, Cr 4.20 *w*/% and Ce 0.07 *w*/%. The alloy was manufactured by vacuum smelting in a foundry furnace, which enables charging through a vacuum forehead. The melting temperature of the material is 1780 K. Cooling was slow, the shells were covered with insulating material after casting. The cast bars were further processed by rolling at high temperatures. The resulting structure of the material is shown in **Figure 1**.

Selected individual data needed for a subsequent temperature analysis were measured in dependence on the temperature. Namely, the specific heat C_p and the thermal conductivity k. The temperature dependence of the thermal conductivity and specific heat is shown in **Figure 2**. Values of these quantities at temperatures in the range 293–1773 K are approximated by the method of least squares, with the aid of the experimentally measured data. For temperatures above 1773 K an approximation by an extrapolation technique is employed.[6] In the case of the temperature dependence of the quantity

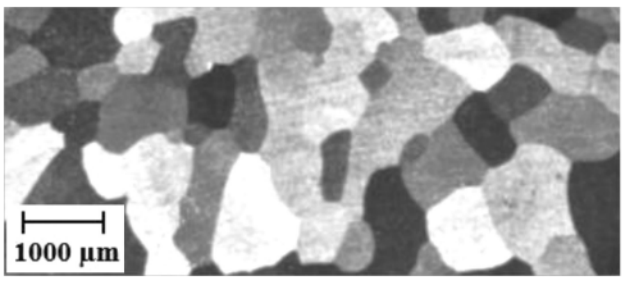

Figure 1: Misrostructure of iron aluminide

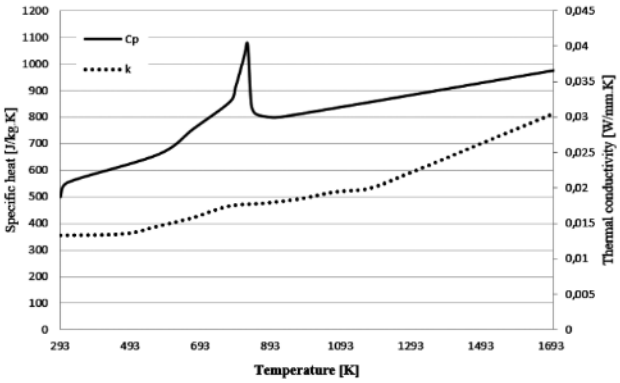

Figure 2: Thermal conductivity and specific heat temperature dependence

C_p it is possible to observe the peak value in the range of the phase transformation of aluminum. On the other hand, the heat-transfer coefficient for the interface of iron aluminide and air of 293 K (i.e., the ambient temperature) under the given conditions is assumed to be constant 20 J/(m^2·K) and the material's surface emissivity is 0.62. Since the density of iron aluminide does not change significantly with temperature, we also consider it as being constant at 6.62 g/cm^3.

3 MATHEMATICAL MODEL

In order to investigate the temperature distribution during the laser-welding process, we have proposed the following model under simplified conditions. We use two flat sheets in a butt joint of Fe_3Al of the same thickness. Since the movement of a laser is considered exactly along the contact line of the top surface, we can assume that the contact of the two flat sheets is ideal, i.e., the whole nominal surface is in contact. This fact implies that we use only one computational domain for a description of the geometry.[7] The second possibility is to employ half of the geometry and add an impermeability condition on the boundary of the joint. This approach cannot be used when laser welding is performed outside of the materials' joint. In that case one has to take into account that the actual contact is significantly smaller than the area of both contacting surfaces and causes a thermal contact resistance.[8]

Further, in the real situation we consider that the work piece is fixed and surrounded by air, while the laser modelled by the heat source moves only in one direction along the contact line with a constant speed. In addition, the laser beam is perpendicular to the top surface of the welded flat sheets and the laser head has a constant distance from this surface throughout the welding process. A mathematical model used to describe the temperature distribution is given by 3D nonlinear heat transfer equation equipped with the appropriate boundary conditions.[9] Moreover, to simplify the whole study we restrict ourselves to a 2D situation in one fixed cross cut of the 3D domain, see **Figure 3** (the contact boundary is not high-

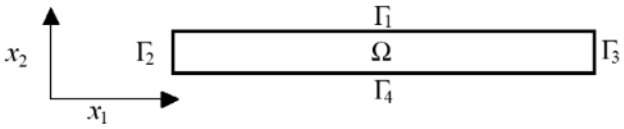

Figure 3: Simulation domain and its boundaries

lighted). As a result, the considered welding direction is perpendicular to the (x_1,x_2) plane. Therefore, we neglect the temperature changes in the moving direction of the laser and introduce a time dependence to the heat fluxes and sources. For more details see Section 5.

Since the thickness (x_2-diameter) of the sheets is much smaller than their width (x_1-diameter), the Dirichlet boundary conditions with constant workpiece temperature are prescribed on the left and right boundaries, whereas the convection heat loss on the top and bottom boundaries is modelled by the Newton cooling law and the Stefan–Boltzmann law is employed to model the radiated energy. In other words, convection and radiation are most enforced on boundary Γ_1 and Γ_4. Furthermore, as is well known, the temperature decreases exponentially with increasing distance from the heat source. Therefore, it is reasonable to prescribe the ambient temperature at the far-field boundaries Γ_2 and Γ_3 see (2). In line with,[9] assuming heat input only on the upper surface of the material might not lead to correct results we thus propose a combination of the surface-distributed heat flux and the volumetric heat-source term to capture the effect of the laser beam, see Section 5. Except for the density the rest of the thermophysical properties of Fe_3Al are considered to be temperature dependent. To summarize the above, we deal with the following nonlinear parabolic partial differential equation

$$\rho C_p(T)\frac{\partial T}{\partial t} - \operatorname{div}(k(T)\nabla T) = f_L(x,t) \quad \text{in } \Omega\times I \tag{1}$$

$$T = T_0 \quad \text{on } (\Gamma_2 \cup \Gamma_3)\times I \tag{2}$$

$$k(T)\frac{\partial T}{\partial x_2} = q_L(x,t) - \sigma\varepsilon(T^4 - T_0^4) - h(T - T_0) \quad \text{on } \Gamma_1 \times I \tag{3}$$

$$-k(T)\frac{\partial T}{\partial x_2} = -\sigma\varepsilon(T^4 - T_0^4) - h(T - T_0) \quad \text{on } \Gamma_4 \times I \tag{4}$$

$$T(x,0) = T_0 \quad \text{in } \Omega\times\{0\} \tag{5}$$

where $I = (0, t_{max})$ denotes the time interval and $x = [x_1,x_2]$ stands for the spatial coordinates of a general point from the simulation domain $\Omega \subset R^2$ (a rectangle) with boundaries Γ_1, Γ_2, Γ_3, Γ_4 as defined in **Figure 3**. Note that if a general geometry of the top and bottom surfaces of the work piece was assumed, the left-hand sides of (3) and (4) would transform to $k(T)\cdot\partial T/\partial n$, where n denotes the outer unit normal vector to the boundary Γ_1 and Γ_4, respectively.

In the formulation (1)–(5) we used the following quantities: $T = T(x,t) > 0$ is the thermodynamic temperature, t is the simulation time, ρ is the material density being considered as a constant, $C_p(T)$ is the material specific heat at the temperature T, $k(T)$ is the material thermal conductivity at the temperature T, T_0 is the constant ambient temperature, $f_L(x,t)$ is the volumetric laser heat source, $q_L(x,t)$ is the surface-distributed laser heat flux, $\sigma = 5.67 \times 10^{-8}$ W/(m^2·K) is the Stefan–Boltzmann constant. Both quantities, the coefficient of convective heat transfer h and the material surface emissivity ε, are again considered as constants, see Section 2.

In order to solve the problem (1)–(5) numerically, we need to derive its weak formulation. Hence, we define the space $V = \{v \in H^1(\Omega), v = 0$ on $\Gamma_2 \cup \Gamma_3$ in the sense of traces$\}$, multiply the equation (1) by any $\varphi \in V$, integrate over the domain Ω and apply Green's theorem. The weak formulation of (1)–(5) then reads: *Find T defined in $\Omega \times I$ such that $T - T_0 \in V$ for almost all $t \in I$ and there holds*

$$\left(\rho C_p(T)\frac{\partial T}{\partial t}, \varphi\right)_\Omega + b(T, T - T_0, \varphi) = F(t,\varphi) \tag{6}$$

for all $\varphi \in V$ and for almost all $t \in I$, where $(\cdot,\cdot)_\Omega$ is the $L^2(\Omega)$ inner product satisfying $(u,v)_\Omega = \int_\omega uv\,dx$ for all $u,v \in L^2(\Omega)$ and

$$b(v,u,\varphi) = (k(v)\nabla u, \nabla\varphi)_\Omega + \int_{\Gamma_1\cup\Gamma_4} (\sigma\varepsilon(v^3 + v^2T_0 + vT_0^2 + T_0^3) + h)u\varphi\,ds \tag{7}$$

$$F(t,\varphi) = (f_L(x,t),\varphi)_\Omega + \int_{\Gamma_1} q_L(x,t)\varphi\,ds \tag{8}$$

Consequently, if we assume $f_L \in L^1(I; L^2(\Omega)) \cup L^2(I; L^p(\Omega))$, $q_L \in L^2(I; L^s(\Gamma_1))$ for some $p,s \in (1, \infty)$, $T_0 \in L^2(\Omega)$ and $0 < k(r)/C_p(r) \le C(1 + \left|\int_0^r C_p(z)dz\right|^q)$, for $q < 2$, we can prove that there is a unique solution $T \in L^2(I; H^1(\Omega)) \cup L^\infty(I; L^2(\Omega))$ with $\partial T/\partial t \in L^1(I; W^{1,\infty}(\Omega)^*)$.[10] For the definition of mentioned Sobolev and Bochner spaces, see the book of Adams and Fournier.[11]

4 NUMERICAL TREATMENT

The numerical methods take a crucial part in the optimization of the laser-welding process. In order to improve the valuation of the temperature field and to resolve significant properties under the studied model more properly, we employ advanced techniques that arise from a variational formulation. Specifically, the discontinuous Galerkin (DG) method (see the book of Dolejší and Feistauer[12] for a complete overview) is used and leads to the construction of a numerical solution (i.e., an approximation of the temperature distribution) as a composition of piecewise polynomial functions over a partitioned domain Ω. Moreover, this discontinuous approach seems to be more advantageous in comparison with the standard finite-element method (FEM), since it enables better resolution and identification of certain non-smooth

structures that can occur during the laser-welding process, e.g., melting boundary.

We propose a numerical algorithm consisting of two consecutive phases – temporal semi-discretization and DG spatial discretization. Within the first phase, we choose $M \in \mathrm{N}$ and define a partition of the interval $I = (0,t_{\max})$ as $0 = t_0 < < \cdots < t_M = t_{\max}$. For simplicity we consider $t_\mathrm{m} = m\tau$, for $m = 0,1,2,\ldots,M$ and $\tau = t_{\max}/M$. If $T^\mathrm{m} \approx T(x,t_\mathrm{m})$ and if we approximate

$$\frac{\partial T}{\partial t}(x,t_{\mathrm{m}+1}) \approx \frac{T^{\mathrm{m}+1}-T^{\mathrm{m}}}{\tau},\ C_\mathrm{p}(T^{\mathrm{m}+1}) \approx C_\mathrm{p}(T^\mathrm{m}) \\ b(T^{\mathrm{m}+1},T^{\mathrm{m}+1}-T_0,\varphi) \approx b(T^\mathrm{m},T^{\mathrm{m}+1}-T_0,\varphi) \tag{9}$$

we obtain for all $\varphi \in \mathrm{V}$ and $m = 0,1,2,\ldots,M-1$ the linearized scheme

$$\left(\rho C_\mathrm{p}(T^\mathrm{m})\frac{T^{\mathrm{m}+1}-T^\mathrm{m}}{\tau},\varphi\right)_\Omega + b(T^\mathrm{m},T^{\mathrm{m}+1},\varphi) = \\ = F(t_{\mathrm{m}+1},\varphi) + b(T^\mathrm{m},T_0,\varphi) \tag{10}$$

Hence, if we denote

$$\mathcal{B}^\mathrm{m}(q,\varphi) = (\rho C_\mathrm{p}(T^\mathrm{m})q,\varphi)_\Omega + \tau b(T^\mathrm{m},q,\varphi) \tag{11}$$

$$\mathcal{F}^\mathrm{m}(\varphi) = (\rho C_\mathrm{p}(T^\mathrm{m})T^\mathrm{m},\varphi)_\Omega + \\ + \tau F(t_{\mathrm{m}+1},\varphi) + \tau b(T^\mathrm{m},T_0,\varphi) \tag{12}$$

we solve a sequence of linear problems in space (so-called Rothe's method): *For each* $m = 0,1,2,\ldots,M-1$ *find a function* $T^{\mathrm{m}+1} \in H^1(\Omega)$ *such that* $T^{\mathrm{m}+1} - T_0 \in V$ *and there holds*

$$\mathcal{B}^\mathrm{m}(T^{\mathrm{m}+1},\varphi) = \mathcal{F}^\mathrm{m}(\varphi) \ \text{ for all } \varphi \in V \tag{13}$$

In the second stage, we solve equations (13) with the aid of the non-symmetric interior penalty variant of discontinuous Galerkin (NIPG) method, introduced, e.g., in the book.[12] Let $\mathcal{T}_\mathrm{h} = \{K\}_{K\in\mathcal{T}_\mathrm{h}}$ be any shape-regular triangulation of the domain Ω and K denotes an element of triangulation. Over $\mathcal{T}_\mathrm{h}$ we define the so-called broken Sobolev space $H^1(\Omega,\mathcal{T}_\mathrm{h}) = \{v|_K \in H^1(K),\ K \in \mathcal{T}_\mathrm{h}\}$ and a finite dimensional space of discontinuous piecewise polynomial functions $S_\mathrm{hp} = S_\mathrm{hp}(\Omega,\mathcal{T}_\mathrm{h}) = \{v \in H^1(\Omega,\mathcal{T}_\mathrm{h}),\ v|_K \in P_\mathrm{p}(K),\ K \in \mathcal{T}_\mathrm{h}\}$. For each $m = 0,1,2,\ldots,M-1$ the DG method then reads: *Find* $T_\mathrm{h}^{\mathrm{m}+1} \in S_\mathrm{hp}$ *satisfying*

$$\mathcal{B}_\mathrm{h}^\mathrm{m}(T_\mathrm{h}^{\mathrm{m}+1},\varphi_\mathrm{h}) + \tau\mathcal{J}_\mathrm{h}(T_\mathrm{h}^{\mathrm{m}+1},\varphi_\mathrm{h}) = \mathcal{F}_\mathrm{h}^\mathrm{m}(\varphi_\mathrm{h})\ \forall\varphi_\mathrm{h} \in S_\mathrm{hp} \tag{14}$$

where the bilinear form $\mathcal{B}_\mathrm{h}^\mathrm{m}$ stands for the DG semi-discrete variant of the form $\mathcal{B}^\mathrm{m}$, whose diffusion part is treated by the NIPG variant of stabilization. Moreover, the penalty form $\mathcal{J}_\mathrm{h}$ is added to the discrete formulation in order to compensate the inter-element discontinuities and to stabilize the resulting numerical scheme. Finally, the right-hand side form $\mathcal{F}_\mathrm{h}^\mathrm{m}$ encompasses terms of the temporal derivative evaluated at the previous time level and terms arising from the boundary conditions. The derivation of the afore-mentioned forms follows the standard steps outlined in the book.[12]

When solving the system of equations (14), we consider the basis $\{v_i\}_{i=1}^N$ of the space S_hp and look for $T_\mathrm{h}^{\mathrm{m}+1} = \sum_{i=1}^N \alpha_i^{\mathrm{m}+1} v_i$. The coefficients $\alpha_i^{\mathrm{m}+1}$ are then solutions of the system of linear equations

$$\sum_{i=1}^N \beta_{ij}^\mathrm{m}\alpha_i^{\mathrm{m}+1} = r_j^\mathrm{m} \quad \text{for } j = 1,2,\ldots,N \tag{15}$$

where $\beta_{ij}^\mathrm{m} = \mathcal{B}_\mathrm{h}^\mathrm{m}(v_i,v_j)$ and $r_j^\mathrm{m} = \mathcal{F}_\mathrm{h}^\mathrm{m}(v_j)$, for $i,j = 1,2,\ldots,N$. Since the supports of the basis functions v_i are small, the system matrix of (15) is sparse and has a block structure. Due to its non-symmetry, the restarted GMRES solver is incorporated into the numerical procedure.

5 SIMULATION RESULTS AND DISCUSSION

The experiment is designed as follows. The size of the plates taken for welding are of 10 mm width, with a thickness of 3 mm, i.e., $|\Gamma_2| = |\Gamma_3| = 3$ mm and $|\Gamma_1| = |\Gamma_4| = 20$ mm. The length of the sheets that would correspond to reality would be long enough to perform the entire simulation by the final time at a given constant welding speed. The whole simulation domain Ω is adaptively meshed with 5980 elements to resolve the temperature distribution more properly in the presumed area of the weld pool and HAZ.

The numerical experiment corresponds to the welding preparation of the samples with an LPSS Nd: YAG Laser. The power of the laser beam P on the welded sample is assumed to be 800–1200 W and the welding speed v in range 6–10 mm/s.

Specifically, we test 9 scenarios for the combinations $P \in \{800,1000,1200\}$ and $v \in \{6,8,10\}$. The aim of the numerical experiments is to optimize the laser's power settings and especially the welding speed. For this purpose, we created a numerical study, which is focused on the analysis of the temperature field during welding. By optimizing the temperature field, it will then be possible to select the optimum welding mode to ensure the best possible welding conditions for the material.

The computation of the temperature field relies essentially on the heat flux/source model that dates back to the pioneering work of Rosenthal.[13] As mentioned above, the moving laser beam is simulated by the combination of surface-distributed heat flux q_L and volumetric heat source f_L. The form of the surface-distributed heat flux originates from the travelling 2D Gaussian pulse[8] that is constructed as a product of two Gaussian distributions in directions related to the width of the sheets and the welding direction, satisfying the condition that three standard deviations of the pulse correspond to the radius of the laser beam $R = 0.45$ mm. In order to capture the movement of the surface-distributed heat flux, the argument of the Gaussian pulse (in the welding direction) has to be shifted by the amount $v(t - t_{\mathrm{mid}})$, where t_{mid} is a user-defined parameter that denotes the time in which the centre of the laser beam in the 3D model would reach the level of the cross cut from the beginning of the simulation. Accordingly, for the studied 2D case, the coordinate in

the welding direction is fixed as the coordinate of the cross cut. Without any loss of generality, we can set it to zero, then the surface-distributed heat flux can be written in the following form

$$q_{\mathrm{L}}(x,t) = P\eta\left(\frac{3}{R\sqrt{2\pi}}\,\mathrm{e}^{-\frac{9x_1^2}{2R^2}}\right)\left(\frac{3}{R\sqrt{2\pi}}\,\mathrm{e}^{-\frac{9\upsilon^2(t-t_{\mathrm{mid}})^2}{2R^2}}\right) \tag{16}$$

where η denotes the absorptivity of Fe_3Al (considered as 0.3). Since q_{L} acts only on Γ_1, it does not depend on the x_2-coordinate.

Subsequently, the form of the volumetric heat source is directly given by a conical extension of (16) in the x_2-direction, determined by the cone radius parameters R and R_{b}, where $R_{\mathrm{b}} = 0.7R$ is the parameter of a Gaussian curve at the bottom boundary Γ_4. More specifically,

$$f_{\mathrm{L}}(x,t) = P\eta\left(\frac{3}{R_0\sqrt{2\pi}}\,\mathrm{e}^{-\frac{9x_1^2}{2R_0^2}}\right)\left(\frac{3}{R_0\sqrt{2\pi}}\,\mathrm{e}^{-\frac{9\upsilon^2(t-t_{\mathrm{mid}})^2}{2R_0^2}}\right) \tag{17}$$

where

$$R_0 = R_0(x_2) = R - (R - R_{\mathrm{b}})\cdot\frac{e_{\mathrm{u}} - x_2}{|\Gamma_2|} \tag{18}$$

and e_{u} stands for the x_2-coordinate of the top boundary Γ_1. The dependence of f_{L} on x_2 is expressed by the relation (18) and we can simply verify that f_{L} on Γ_1 (i.e., for $x_2 = e_{\mathrm{u}}$) is consistent with q_{L}.

In order to perform the numerical experiments, the proposed numerical scheme is implemented in the solver Freefem++, for more details to a mesh generation/adaptation, the spatial and temporal discretization, the assem-

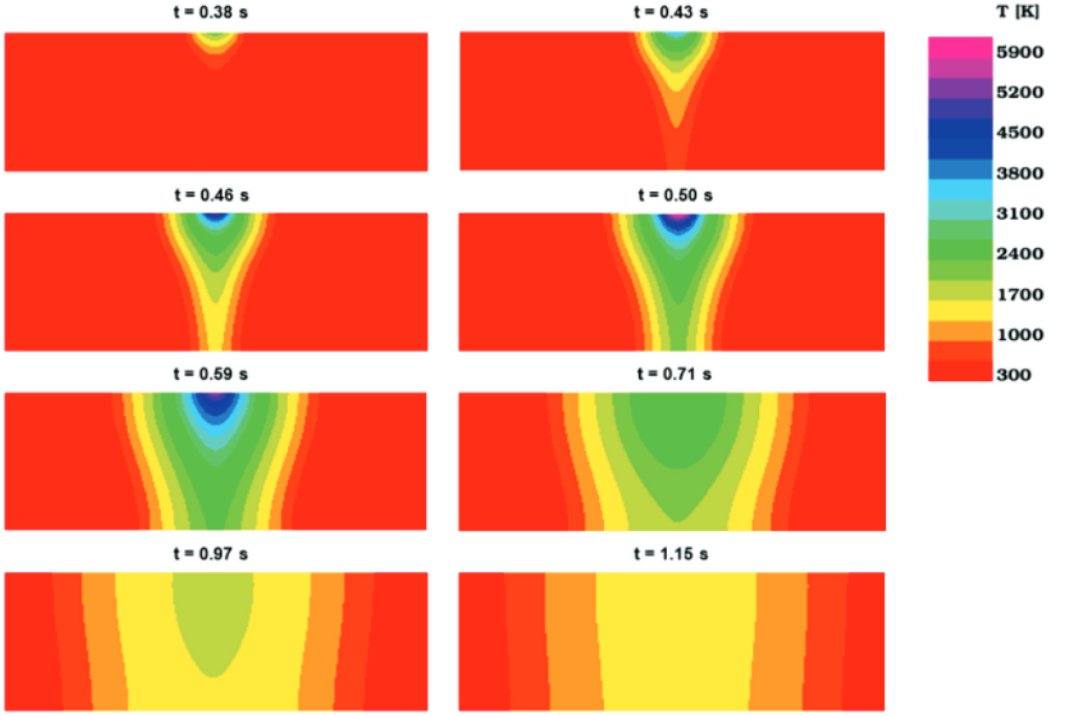

Figure 4: Temperature distribution in the domain Ω at eight different time instants for the welding parameters: P = 1000 W and v = 8 mm/s

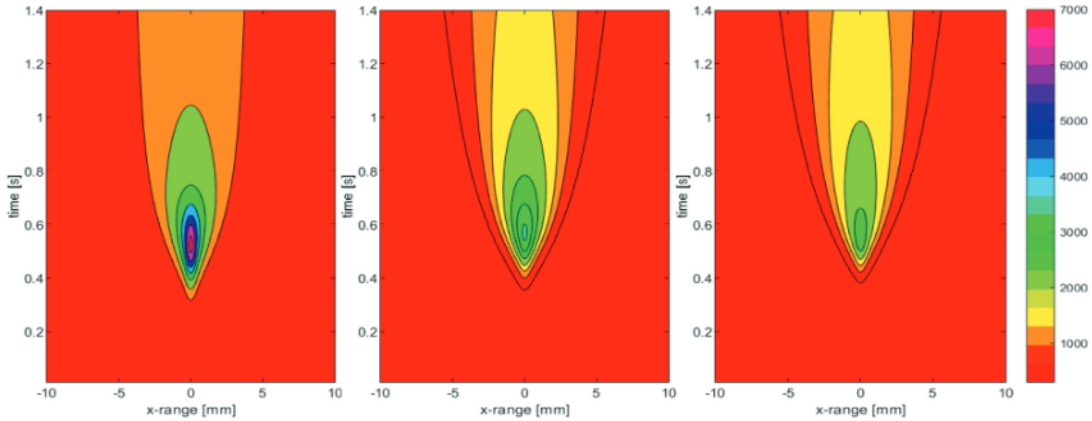

Figure 5: Temperature field in (x_1,t) plane at three layers: upper (left), middle, bottom (right)

bly of a linear algebraic problem and its solving, see paper.[14] For all the scenarios we compute the piecewise linear (i.e., $p = 1$) numerical solutions on a fixed grid. The time step is fixed sufficiently small as $\tau = 0.01$ to suppress the influence of the time discretization on the results and the final time of the simulation is equal to $t_{max} = 3$ s.

Figure 4 plots isothermal charts for a particular scenario of the welding process at eight selected time instants to capture the development of the temperature distribution from the initiation of the process, over peak temperature values to the material cooling phase. Accordingly, we can easily observe the formation and the shape of the resulting weld pool with a maximum temperature of 7273 K. For better imagination, we also append charts illustrating continuously the time dependence of the temperature distribution across the frontal cut at three selected layers (upper Γ_1, middle and bottom Γ_4) for the same welding parameters ($P = 1000$ W and $v = 8$ mm/s), see **Figure 5**. The interested reader can see that these results are in a good agreement with the preceding observations. Moreover, we can easily obtain a 3D plot of the temperature distribution during the whole simulation by a simple combination of outputs from **Figure 4** and **Figure 5**.

To conclude the experiment, we try to localize the weld pool at the fixed time instant by the identification of the boundary with the melting temperature of Fe_3Al, well-known as the fusion line. Therefore, our aim is to determine the distance of the centre of the weld and the fusion line at three selected layers (upper, middle and bottom). The observed results in millimetres for all scenarios at time $t = t_{mid} = 0.5$ s are listed in **Table 1**.

Table 1: Distances (in mm) of the centre of the weld and the fusion line at upper, middle and bottom layers for various welding parameters

v[mm/s]	P[W]		
	800	1000	1200
6	1.143	1.270	1.373
	0.684	0.848	0.976
	0.411	0.568	0.692
8	1.061	1.179	1.276
	0.579	0.733	0.855
	0.333	0.479	0.594
10	1.001	1.115	1.205
	0.506	0.652	0.768
	0.278	0.419	0.528

The order of values in cells (**Table 1**) corresponds to upper, middle and bottom layer subsequently. These observations are in good agreement with expected behavior when the size of the molten zone increases with the higher power of a laser beam and a decreasing welding speed. The data in the table make it possible to predict the size and shape of the molten zone for a different set of welding parameters such as laser power and welding speed. It is thus possible to get an idea of the level of influence of the changes when adjusting one or both parameters. With a larger number of data, it would then be possible to predict in what proportion, when changing the welding speed, it is necessary to adjust the power of the source to achieve the desired profile of the weld pool. In other words, it would be possible to determine heuristically in what ratio P/v these quantities should be in order to preserve the shape of the molten zone.

6 CONCLUSIONS

Based on the presented mathematical model, the proposed numerical approach and the analysed experimental results, the following conclusions can be drawn:

- The restriction of the 3D model of laser welding to a 2D case has its justification, as it leads to obtaining relevant results, while reducing the computational complexity.
- It has been also confirmed that in this type of welding, it is desirable to use a combination of surface and volumetric heat source to model the laser effect.
- The numerical scheme based on the DG method showed its potential in the given issue.
- The observed experimental results illustrate a number of aspects, including the shape and size of the molten area depending on the setting of the welding parameters.
- To summarize, we present an alternative tool for the optimization of a laser-welding process under certain simplified conditions. The advantages of this numerical study are especially apparent for the case of Fe_3Al, which is a material difficult to manufacture and process, and thus the possibilities of its real experimental tests are significantly limited.

Acknowledgment

The research was partially supported by the project No. PURE-2020-4003 financed by Technical University of Liberec, and by project No. CZ.02.1.01/0.0/0.0/16_019/0000778 financially supported by the European Regional Development Fund (Center of Advanced Applied Sciences – CAAS). The support is greatly acknowledged.

7 REFERENCES

[1] J. H. DeVan, Oxidation Behavior of Fe3Al and Derivative Alloys, Oxidation of High-Temperature Intermetallics (T. Grobstein and J. Doychak, eds.), 1989, 107

[2] C. McKamey, J. DeVan, P. Tortorelli, V. Sikka, A review of recent developments in Fe3Al-based alloys. Journal of Materials Research, 6 (**1991**) 8, 1779–1805, doi:10.1557/JMR.1991.1779

[3] S. C. Deevi, V. K. Sikka, Nickel and iron aluminides: an overview on properties, processing, and applications, Intermetallics, 4 (**1996**) 5, 357–375, doi:10.1016/0966-9795(95)00056-9

[4] Y. Nishino, S. Asano, T. Ogawa, Phase stability and mechanical properties of Fe_3Al with addition of transition elements, Materials Science and Engineering A-structural Materials Properties Micro-

structure and Processing, 234 (**1997**), 271–274, doi:10.1016/S0921-5093(97)00191-3

[5] A. A. Fasching, D. I. Ash, G. R. Edwards, S. A. David, Hydrogen cracking behavior in an iron aluminide alloy weldment, Scripta Metallurgica et Materialia, 32 (**1995**) 3, 389–394, doi:10.1016/S0956-716X(99)80070-3

[6] J. Bradáč, Determination of the welding process of iron aluminide with the support of simulation calculations in the SYSWELD program, Technical university of Liberec, Liberec 2009, 154 p.

[7] U. Kumar, D. K. Gope, J. P. Srivastava, S. Chattopadhyaya, A. K. Das, G. Krolczyk, Experimental and numerical assessment of temperature field and analysis of microstructure and mechanical properties of low power laser annealed welded joints, Materials (Basel), 11 (**2018**) 9, 1514, doi:10.3390/ma11091514

[8] S. D'Ostuni, P. Leo, G. Casalino, FEM Simulation of Dissimilar Aluminum Titanium Fiber Laser Welding Using 2D and 3D Gaussian Heat Sources, Metals, 7 (**2017**) 8, 307, doi:10.3390/met7080307

[9] K. R. Balasubramanian, N. Siva Shanmugam, G. Buvanashekaran, K. Sankaranarayanasamy, Numerical and experimental investigation of laser beam welding of AISI 304 stainless steel sheet, Advances in Production Engineering & Management, 3 (**2008**) 2, 93–105

[10] T. Roubíček, Nonlinear Partial Differential Equations with Applications, International Series of Numerical Mathematics 153, Birkhäuser Basel, 2013, 476, doi:10.1007/978-3-0348-0513-1

[11] R. Adams, J. Fournier, Sobolev Spaces, 2nd ed., Academic Press, New York, 2003, 320

[12] V. Dolejší, M. Feistauer, Discontinuous Galerkin Method: Analysis and Applications to Compressible Flow, Springer Series in Computational Mathematics 48, Springer International Publishing, 2015, 572, doi:10.1007/978-3-319-19267-3

[13] D. Rosenthal, Mathematical theory of heat distribution during welding and cutting, Welding Journal, 20, (**1941**), 220–234

[14] F. Hecht, New development in FreeFem++, Journal of Numerical Mathematics, 20 (**2012**), 251–265